HHS Public Access

Author manuscript

Cancer Discov. Author manuscript; available in PMC 2021 July 01.

Published in final edited form as:

Cancer Discov. 2021 January ; 11(1): 126–141. doi:10.1158/2159-8290.CD-20-0571.

TRK xDFG mutations trigger a sensitivity switch from type I to II kinase inhibitors

Emiliano Cocco[1,2,†], **Ji Eun Lee**[*,3], **Srinivasaraghavan Kannan**[*,4], **Alison M Schram**[*,5,6], **Helen H Won**[7], **Sophie Shifman**[1,2], **Amanda Kulick**[8], **Laura Baldino**[1,2], **Eneda Toska**[1], **Amaia Arruabarrena-Aristorena**[1], **Srushti Kittane**[1], **Fan Wu**[1], **Yanyan Cai**[1], **Sabrina Arena**[9,10], **Benedetta Mussolin**[10], **Ram Kannan**[3], **Neil Vasan**[1], **Alexander N. Gorelick**[1,11], **Michael F Berger**[1,2,7], **Ofra Novoplansky**[12], **Sankar Jagadeeshan**[12], **Yi Liao**[13], **Uwe Rix**[13], **Sandra Misale**[14], **Barry S Taylor**[11], **Alberto Bardelli**[9,10], **Jaclyn F Hechtman**[2], **David M Hyman**[5,6], **Moshe Elkabets**[12], **Elisa de Stanchina**[8], **Chandra S Verma**[4,15,16,†], **Andrea Ventura**[3,†], **Alexander Drilon**[5,6,†], **Maurizio Scaltriti**[1,2,†]

[1]Human Oncology and Pathogenesis Program, Memorial Sloan Kettering Cancer Center, New York, NY 10065, US

[2]Department of Pathology, Memorial Sloan Kettering Cancer Center, New York, NY 10065, US

[3]Cancer Biology and Genetics Program, Memorial Sloan Kettering Cancer Center, New York, NY 10065, US

[4]Bioinformatics Institute (BII), Agency for Science, Technology and Research (A*STAR), Singapore

[5]Department of Medicine, Memorial Sloan Kettering Cancer Center, New York, NY 10065, US

[6]Weill Cornell Medical College, New York, NY 10065, US

[7]Center for Molecular Oncology, Memorial Sloan Kettering Cancer Center, New York, NY 10065, US

[8]Antitumor Assessment Core Facility, Memorial Sloan Kettering Cancer Center, New York, NY 10065, US

[9]Department of Oncology, University of Torino, Candiolo (TO) 10060, Italy

[10]Candiolo Cancer Institute, FPO-IRCCS, Candiolo (TO) 10060, Italy

[†] Corresponding authors Maurizio Scaltriti (Lead contact): Memorial Sloan Kettering Cancer Center, Room Z-1702, 1275 York Avenue, Box 20, New York, NY 10065; Tel: 6468883519; Fax: 6464220247; scaltrim@mskcc.org, Emiliano Cocco: Memorial Sloan Kettering Cancer Center, Room Z-1702, 1275 York Avenue, Box 20, New York, NY 10065; Tel: 6468882721; coccoe@mskcc.org, Chandra S Verma: #07-38, level 7 Matrix (Biopolis), Bioinformatics Institute, A*STAR Singapore. Tel: (65)-6478-8273; chandra@bii.a-star.edu.sg, Andrea Ventura: Memorial Sloan Kettering Cancer Center, Zuckerman Research Laboratory, 417 East 68th Street, New York, NY 10065; Tel: 646-888-3068; Fax: 646-422-0871; venturaa@mskcc.org, Alexander Drilon: Memorial Sloan Kettering Cancer Center, 885 Second Ave, New York, NY 10017; Tel: 646-608-3758; drilona@mskcc.org.

[*]Equal contribution

AUTHORS' CONTRIBUTIONS

E.C., J.E.L., S.K., A.M.S., C.S.V., A.V., A.D. and M.S. conceived the study. S.K. and C.S.V. discussed the modelling experiments and analyses, S.K. carried out the modelling experiments. H.H.W., A.N.G., J.F.H. and M.F.B. analyzed DNA and RNA sequencing. E.C., J.E.L., S.S., A.K., L.B., E.T., A.A.A., S.A., B.M., R.K., N.V., O.N., S.J., M.E., Y.L., U.R., A.B. and E.d.S. designed biochemical assays and performed cell-based and in vivo experiments. E.C., A.M.S., D.M.H., A.V., A.D. and M.S. wrote the manuscript with input from all authors.

[11]Department of Epidemiology and Biostatistics, Memorial Sloan Kettering Cancer Center, New York, NY 10065 US

[12]The Shraga Segal Department of Microbiology, Immunology, and Genetics, Faculty of Health Sciences, Ben-Gurion University of the Negev, 84105 Beer-Sheva, Israel

[13]Department of Drug Discovery, Moffitt Cancer Center, 33612, Tampa, FL

[14]Molecular Pharmacology Program, Memorial Sloan Kettering Cancer Center, New York, NY

[15]School of Biological Sciences, Nanyang Technological University, 637551, Singapore

[16]Department of Biological Sciences, National University of Singapore, 117543, Singapore

Abstract

On-target resistance to next-generation TRK inhibitors in TRK fusion-positive cancers is largely uncharacterized. In patients with these tumors, we found that TRK xDFG mutations confer resistance to type I next-generation TRK inhibitors designed to maintain potency against several kinase domain mutations. Computational modeling and biochemical assays showed that TRKA G667 and TRKC G696 xDFG substitutions reduce drug binding by generating steric hindrance. Concurrently, these mutations stabilize the inactive (DFG-out) conformations of the kinases, thus sensitizing these kinases to type II TRK inhibitors. Consistently, type II inhibitors impede the growth and TRK-mediated signaling of xDFG-mutant isogenic and patient-derived models. Collectively, these data demonstrate that adaptive conformational resistance can be abrogated by shifting kinase engagement modes. Given the prior identification of paralogous xDFG resistance mutations in other oncogene-addicted cancers, these findings provide insights into rational type II drug design by leveraging inhibitor class affinity switching to address recalcitrant resistant alterations.

Keywords

NTRK fusions; xDFG mutations; conformational resistance; type II inhibitors; 2nd-generation TRK inhibitors

INTRODUCTION

Sequential tyrosine kinase inhibitor (TKI) therapy is an established strategy for cancers driven by an oncogenic kinase (1). Treatment is initiated with an early-generation TKI and, upon the acquisition of resistance, a next-generation TKI is employed. This paradigm is typified by fusion-positive cancers for which rationally-designed next-generation TKIs (lorlatinib for ALK fusions; repotrectinib for ROS1 fusions) have been shown to re-establish disease control in the face of kinase domain mutation-mediated resistance to earlier-generation inhibitors (crizotinib, ceritinib or alectinib for ALK fusions; crizotinib or entrectinib for ROS1 fusions) (2–4). The design of these next-generation agents is informed by a wealth of information on mechanisms that drive resistance to early-generation therapy (5).

Unfortunately, the dynamics that drive resistance to next-generation TKI therapy are more poorly characterized. In particular, while the evolutionary pressures of sequential TKI therapy propel the emergence of off-target/bypass tract-mediated resistance in select cancers (4,6), other cancers clearly acquire on-target resistance. On-target resistance mechanisms must induce structural changes in the kinase domain that ultimately impair the inhibitory effects of drug binding but simultaneously maintain kinase activity. Identifying and characterizing these mechanisms is an unmet need.

TRK fusion-positive cancers provide a prototype for the study of persistent on-target resistance in the context of sequential TKI therapy across lineage climates (7). First-generation TRK inhibitors such as larotrectinib and entrectinib are approved by multiple regulatory agencies for the treatment of TRK fusion-positive adult and pediatric cancers in a tumor-agnostic fashion (8–10). In response to first-generation therapy, many cancers will acquire kinase domain mutations that mediate resistance (8,11,12). Interestingly, these mutations result in amino acid substitutions in conserved regions that are paralogous to kinase domain substitutions that mediate resistance in other fusion-positive cancers. For example, the solvent front substitutions TRKA G595R and TRKC G623R are paralogous to ALK G1202R and ROS1 G2032R (4). The 2nd-generation TRK inhibitors selitrectinib (LOXO-195, a selective TRK inhibitor) and repotrectinib (TPX-0005, a multikinase TRK and ROS1 inhibitor) were designed to target many of these kinase domain mutations (13,14). Both drugs are in prospective trials and have shown clinical activity in TRK fusion-positive cancers with kinase domain mutation-mediated resistance to the 1st-generation agents larotrectinib or entrectinib.

In this paper, we study how TRK xDFG mutations can mediate resistance to 2nd-generation TRK inhibitors. The xDFG residue maps immediately N-terminal to the DFG motif, an evolutionary conserved triad across most kinases whose orientation defines the conformational states adopted by kinases (15). In an active or DFG-in conformation, the aspartate (D) of this motif points towards the ATP binding site where it coordinates two Mg^{2+} ions. In the inactive or DFG-out state, the aromatic ring of the phenylalanine (F) residue flips by approximately 180°, moving the aspartate away from the ATP pocket with the consequent inhibition of catalytic activity (15). Small molecule kinase inhibitors that bind to the active conformation of kinases (i.e., 1st- and 2nd-generation TRK inhibitors available in the clinic) are classified as type I inhibitors and are canonical ATP competitors. In addition to the ATP-binding pocket, type II inhibitors also occupy an adjacent allosteric site (commonly referred to as the “back pocket”) across the DFG motif; this back pocket is fully accessible only when the kinases are in the inactive conformation (16,17).

Our study indicates that while TRK xDFG substitutions represent a shared liability for type I TRK inhibitors, these substitutions represent a potential biomarker of sensitivity for type II multikinase inhibitors, drugs that bind to and stabilize the inactive conformations of TRK kinases and prevent their transition into the active state (17,18).

RESULTS

TRKA xDFG Mutations Emerge with Second-generation TRK Inhibitor Resistance

TRKA xDFG mutations resulting in G667 substitutions emerged in tumor DNA from patients with TRK fusion-positive cancers that progressed on 2nd-generation TRK inhibitor therapy (Figure 1). Patient 1, with a *TPM3-NTRK1*-fused, TRKA G595R-mutant sarcoma, was treated with selitrectinib with limited durability. After 4 months of therapy, tumor sequencing at progression (pre- and post-selitrectinib samples obtained from the same lung metastasis site) showed the acquisition of a TRKA G667C (29% allele frequency) mutation and loss of the TRKA G595R solvent front mutation (Figure 1A). Patient 2, with a *LMNA-NTRK1*-fused, TRKA G595R-mutant breast cancer, experienced a mixed response with selitrectinib. Cell-free DNA (cfDNA) collected after two months on therapy (coinciding with rapid liver metastases growth) similarly demonstrated TRKA G667C acquisition and TRKA G595R loss (Figure 1B). For Patient 1, TRKA G667C was found in the pre-treatment sample at 0.3% (2/544 reads). Although the same analysis was not possible for Patient 2, these results suggest that pre-existing TRKA G667C-containing clones may have been selected by selitrectinib treatment.

Patient 3 with an *LMNA-NTRK1*-fused, TRKA G595R-mutant colorectal cancer (CRC) received selitrectinib and developed resistance after 11 months of treatment. Sequencing of the resistant tumor revealed a new TRKA G667A mutation and persistence of the TRKA G595R mutation (Figure 1C). These mutations were clonal, had similar allele frequencies (33% and 27%, respectively), and were found on the same allele in *cis* by RNA sequencing (Supplementary Figure S1A). In parallel, in a TRKA G595R-mutant CRC cell line that became resistant to repotrectinib after continuous drug exposure, we found that a new TRKA G667C substitution was acquired while TRKA G595R was retained (Figure 1D). The allele frequencies of these mutations were similar (63% and 65%, respectively) and RNA sequencing confirmed their occurrence in *cis* (Supplementary Figure S1B). Proliferation assays and Western blot experiments conducted on this cell line showed that 2nd-generation drugs failed to inhibit cell growth and TRK activated downstream signaling, confirming its resistant phenotype (Figure 1E, F).

Given that TRKA G667 mutations were identified at the time of progression on 2nd-generation TRK inhibitor therapy, we sought to evaluate whether these substitutions also confer primary resistance to the same agents. We identified two patients (Patients 4 and 5) who progressed on larotrectinib by acquiring TRKA G667 mutations. Patient 4 with a *TPR-NTRK1*-positive non-small cell lung cancer had a partial response (PR) on larotrectinib. Sequencing of cfDNA at progression identified the emergence of TRKA G667S. Unfortunately, intrinsic resistance to selitrectinib was observed (received only 2 months of therapy; Supplementary Figure S2A). Patient 5, with a *TPM3-NTRK1* positive thyroid cancer, initially responded to larotrectinib and sequencing of the cfDNA at progression identified multiple emergent TRKA kinase mutations, including TRKA G667C and TRKA G667S. Similar to Patient 4, Patient 5 did not respond to selitrectinib (Supplementary Figure S2B). Together, these clinical and preclinical findings suggest that TRKA xDFG

substitutions (as single or compound mutations) limit sensitivity to 2nd-generation TRK inhibitors.

TRKA xDFG Substitutions Compromise 2nd-generation TRK Inhibitor Binding

To investigate the mechanism by which TRKA G667 substitutions confer resistance to 2nd-generation TRK inhibitors, we performed *in silico* molecular modeling combined with molecular dynamics (MD) simulations. Both 2nd-generation TRK inhibitors currently in clinical testing, selitrectinib and repotrectinib, bind to the ATP binding pocket of TRKA with an orientation that places their rigid fluoropyrimidine-containing aromatic moieties in close proximity to the glycine 667 residue. As such, substitution of the small glycine residue with any other amino acid, even those that have side chains with minimal additional bulk (e.g. the methyl side chain for alanine or the thiol side chain for cysteine), results in steric hindrance and compromises selitrectinib and repotrectinib binding (Figure 2A). Consistently, binding free energy calculations indicate that both selitrectinib and repotrectinib lose affinity for TRKA xDFG mutants when compared with wild type TRKA (Supplementary Figure S3A).

To confirm that TRKA G667 mutations result in a reduced activity of 2nd-generation TRK inhibitors, we performed *in vitro* kinase assays using TRKA wild type (WT), TRKA G595R-solvent-front-mutant and TRKA G667-mutant kinases in the presence of increasing concentrations of selitrectinib or repotrectinib. Assays conducted on single (TRKA G667C) and double xDFG mutants (TRKA G595R/G667A and TRKA G595R/G667C) showed that the calculated IC_{50} for selitrectinib was 429.7- to 8514.3-fold higher compared to the IC_{50} obtained against the TRKA WT and 12.3 to 238.4-fold higher compared to the IC_{50} obtained against the selitrectinib-sensitive TRKA G595R solvent front mutant (Figure 2B). Similarly, the calculated IC_{50} for repotrectinib against TRKA xDFG mutants were 59.1- to 1863.6-fold higher compared to the IC_{50} obtained with the TRKA WT and 2.1- to 66.1-fold higher than IC_{50} calculated for the repotrectinib-sensitive TRKA G595R solvent front mutant (Figure 2B). Together, these data indicate that TRKA xDFG mutations limit the sensitivity to selitrectinib and repotrectinib through impaired drug binding.

Type II TRK Inhibitors Preferentially Bind to and Inhibit TRKA, TRKC and ROS1 xDFG Mutants

Existing data suggest that multikinase type II inhibitors can bind TRKA carrying the G667C substitution (19,20). Therefore, we modeled TRKA xDFG and solvent front mutants in complex with three type II inhibitors: cabozantinib, foretinib and ponatinib (21,22). Molecular dynamics simulations and binding free energy calculations suggest that type II drugs can potentially bind the solvent front as well as all the xDFG single and double mutant proteins as the resultant substitutions are not predicted to generate steric hindrance (Figure 3A and Supplementary Figure S3B). Surprisingly, however, *in vitro* kinase assays showed that IC_{50} calculated for cabozantinib, foretinib and ponatinib for TRKA xDFG single and double mutants were 3.4- to 579.3-fold lower than IC_{50} for the solvent front mutant and up to 72.3-fold lower than IC_{50} for TRKA wild type (Figure 3B–D), indicating that the presence of a TRKA xDFG substitution is sufficient to sensitize TRKA kinases to type II inhibitors. Interestingly, mutants with the Gly to Cys substitution in the xDFG codon of the

TRKA kinases were found to be more sensitive to type II inhibitors than the double mutant harboring the Gly to Ala substitution, suggesting allele-specific sensitivity. Together, these results indicate that type II multikinase inhibitors may have higher affinity than type I 2nd-generation TRK specific inhibitors for TRKA xDFG mutants.

To test this hypothesis, we performed *in vitro* microscale thermophoresis to directly measure the binding affinity of cabozantinib/foretinib versus selitrectinib for the TRKA G667C-mutant kinase. Our results show that the dissociation constants (Kds) for cabozantinib and foretinib were 8.84- and 10.74-fold lower than the Kd determined for selitrectinib, respectively (Figure 3E). This suggests that TRKA xDFG substitutions may induce preferential adoption of the DFG-out conformation and increase type II inhibitor binding affinity, similar to data previously reported for the ERK2 kinase modified to harbor xDFG substitutions in mutagenesis-based assays (23). We then carried out all atom MD simulations of apo TRKA in its WT and mutant states. This analysis showed that, in the inactive conformation of the WT TRKA kinase, the xDFG residue (Gly667) is predicted to interact with the side chain of His648 of the His-Arg-Asp (HRD) motif that precedes the activation loop. Due to the flexibility of the Gly667 residue, this interaction is predicted to be weak, facilitating the transition of the TRKA WT kinase from the inactive to the active conformation (Figure 3F, upper panel). When Gly667 is substituted with a Cys, the presence of the bulky side chain group at this position is predicted to bring the carbonyl backbone of Cys667 and the side chain of the His648 into close proximity, thus stabilizing their interaction and favoring the inactive conformation. The distance between Gly667 and His648 in the WT TRKA in the inactive state is about 8 Angstroms but reduces to approximately 3 Angstroms when the Gly667 is substituted with the bulkier Cys (Figure 3F lower panel and Supplementary Figure S3C). According to this model, the reduced flexibility of the Cys667-His648 complex would increase the propensity of the mutated kinase to be stabilized in the inactive state (DFG-out), thus increasing the ability of cabozantinib and foretinib to bind the hydrophobic allosteric back pocket.

To study the generalizability of our findings, we next evaluated whether xDFG mutations also confer sensitivity to type II drugs in another member of the TRK kinases, TRKC, and in ROS1, a kinase that shares 39% identity with TRKA and can also form oncogenic fusions (24). *In vitro* radiometric assays showed that TRKC xDFG (G696A and G696C) and ROS1 xDFG (G2101A and G2101C) mutant recombinant kinases are exquisitely sensitive to type II inhibitors, drugs found to be less active against TRKC and ROS1 wild type or TRKC and ROS1 solvent front (G623R and G2032R, respectively) mutant kinases (Supplementary Figure S4A, B).

Consistent with the biochemical assays, while cabozantinib slightly inhibited TRKC or ROS1 wild type kinase phosphorylation when transfected in HEK293T cells, it markedly inhibited TRKC or ROS1 mediated signaling when the same cells were transfected with the Gly to Cys xDFG TRKC or ROS1 mutants (Supplementary Figure S4C, D). Atom MD simulations of apo TRKC and ROS1 in their WT and mutant states also showed that the distance between the TRKC or ROS1 xDFG residue and the His677/1247 of the HDR motifs reduced about 3-fold when the Gly 696/2101 are substituted with the bulkier Cys

(Supplementary Figure S4E, F). This is predicted to stabilize the mutated kinases in the DFG-out conformation, thus sensitizing to type II agents.

Since our data suggested that xDFG mutations induce structural changes that sensitize to type II drugs in multiple related kinases, we evaluated the prevalence of these mutations in the MSK-IMPACT cohort in 13 kinases that share high sequence identity with TRKA/B/C. Our analysis shows that xDFG mutations are recurrently found in several kinases including RET, ALK, ROS1, EGFR and ERBB2 in tumors of various histology, thus broadening the potential clinical relevance of our findings (Supplementary Figure S4G).

xDFG-Mutant *Bcan-Ntrk1*-Containing Mouse Gliomas Respond to Type II TRK Inhibitors

To test whether type II TRK inhibitors are effective against TRKA xDFG mutants in cell models, we used clustered regularly interspaced short palindromic repeats (CRISPR)-Cas9 to knock-in TRKA solvent front and xDFG single and double mutations in tumor cells derived from a *Bcan-Ntrk1*-driven mouse model of glioma (Supplementary Figure S5; (25)). Single and double mutant clones bearing the Trka G598R solvent front mutation, the mouse orthologue to human TRKA G595R, and/or the Trka G670C/A xDFG substitutions, orthologues to human TRKA G667C/A, (Figures 4A–D, Supplementary Figure S6A–J) were tested for their sensitivity to type I and type II TRK inhibitors. Consistent with our *in vitro* radiometric assays, *Bcan-Ntrk1*, Trka xDFG single and double (xDFG and solvent front) mutant cells were resistant to selitrectinib and repotrectinib, but sensitive to cabozantinib, foretinib, and ponatinib (Figure 4E). Furthermore, type II drugs efficiently inhibited Trka-mediated downstream signaling of Trka single and double xDFG-mutant clones (Figure 4F). Similar results were obtained with two independent clones for each mutant (Supplementary Figure S7A, B).

Resistance to selitrectinib and repotrectinib was reduced in xDFG mutants harboring the Gly to Ala substitution (Trka double-mutant clones). These clones also displayed an intermediate sensitivity to cabozantinib, foretinib and ponatinib, thus paralleling the kinase assay data obtained with this mutant. To further characterize the effect that the TRKA G595R/G667A double mutant has on drug response, we treated mouse glioma cells harboring this double mutation with increasing concentrations of selitrectinib or cabozantinib for 30 minutes or 24 hours and evaluated changes in the phosphorylation status of Trka. Our results showed that, while both drugs were highly effective in inhibiting Trka phosphorylation after 30 minutes of exposure, only cabozantinib maintained efficacy after 24 hours (Supplementary Figure S7C). These data indicate that cabozantinib results in more durable pathway inhibition when compared to selitrectinib in the Trka G598R/G670A double mutant, suggesting that cabozantinib may be more effective than selitrectinib in a chronic regimen or an *in vivo* setting.

To obtain mechanistic insights that could explain why type II inhibitors have increased activity specifically for TRK xDFG mutants, we set to investigate the biochemical properties of Trka xDFG mutant glioma cells. Proliferation and colonies formation assays showed no differences in growth rate or oncogenic potential between cells harboring only the *Bcan-Ntrk1* fusion and cells that also bear the Trka G670C mutation. Cells harboring the solvent front G598R single mutation and cells with the double mutations, Trka G598R/G670A and

Trka G598R/G670C were instead significantly slower and significantly less oncogenic than cells harboring the fusion only or cells also bearing the Trka G670C (Supplementary Figure S7D, E). Together, these data indicate that the increased sensitivity that xDFG single and double mutant cells show for type II inhibitors when compared to cells harboring the fusion only or with the Trka G598R solvent front mutation is not the result of differences in the proliferation rate or the oncogenic properties of these mutants.

We then tested the antitumor activity of type II drugs in *Bcan-Ntrk1*, Trka xDFG-mutant cells injected intracranially into immunocompromised mice. One week after injection, we randomized mice into two groups and performed brain magnetic resonance imaging (MRI). One group (n=3) was treated with vehicle and the other group (n=4) with cabozantinib. We chose cabozantinib as a representative type II TRK inhibitor because of its ability to cross the blood-brain-barrier (BBB) (26). MRI scans after 7 days of treatment showed that, while the tumor size of vehicle-treated mice increased up to 10-fold (accompanied by cerebral edema), cabozantinib prevented tumor growth (Figure 4G, H). Accordingly, mice in the cabozantinib group survived significantly longer than mice in the control group (median of 8 vs 22 days, respectively; P=0.0143; Figure 4I).

Type II TRK Inhibitors Overcome xDFG-mediated Resistance in Patient-derived Models

We next tested the antitumor activity of type II inhibitors in patient-derived models that became resistant to 2nd-generation TRK inhibitors by acquiring TRKA xDFG mutations. Cell proliferation assays showed that these agents are highly active in inhibiting cell growth of the *LMNA-NTRK1*, TRKA G595R/G667C repotrectinib-resistant cell line (described in Figure 1D–F) obtained following chronic drug exposure, while they are significantly less effective against the *LMNA-NTRK1*, TRKA G595R parental counterpart (Figure 5A). In agreement with this phenotype, type II but not type I drugs fully inhibited TRKA downstream signaling in this cell model (Figure 5B).

To confirm that the activity of the type II multikinase inhibitors against the double mutant cell line is the result of the specific inhibition of TRKA and not other targets, we tested the effects of crizotinib (MET inhibitor) and axitinib (VEGFR inhibitor) on cell viability and signaling. Results showed that only type II TRK inhibitors can induce cell death and inhibit TRKA-mediated signaling in the *LMNA-NTRK1*, TRKA G595R/G667C cell line (Supplementary Figure S8A, B). Similarly, xenografts derived from this cell line demonstrated that cabozantinib treatment was sufficient to inhibit tumor growth (Figure 5C).

Lastly, we tested the efficacy of this type II inhibitor in patient-derived xenografts (PDXs) established from the selitrectinib-resistant tumors of Patient 1 (the *TPM3-NTRK1*, TRKA G667C sarcoma) and Patient 3 (the *LMNA-NTRK1*, TRKA G595R/G667A CRC). Patient 1-derived tumors treated with cabozantinib achieved a complete and durable (3 months) response (Figure 5D), while durable (2 months) disease control was observed in tumors derived from Patient 3 (Figure 5E). Taken together, these data indicate that type II TRK inhibitors can overcome acquired resistance to 2nd-generation type I inhibitors mediated by the acquisition of xDFG mutations.

DISCUSSION

The emergence of on-target mutations that predispose oncogenic kinases to switch conformational states is a largely underappreciated mechanism of targeted therapy resistance. Here, we demonstrate that xDFG mutations are recurrently identified in patients and preclinical models from diverse histologies of TRK fusion-positive cancers refractory to 2nd-generation TRK inhibitor therapy. Clones with xDFG mutations can either be present de novo or be acquired with TKI therapy.

Structural modeling and biochemical studies reveal that xDFG substitutions not only limit TRK inhibitor binding by generating steric hindrance but result in preferential adoption of the inactive DFG-out conformation by TRK kinases. Our experiments show that neither differences in growth rate nor the oncogenic potential of these xDFG mutants can explain DFG-out conformation adoption. We thus posit that xDFG substitutions induce structural changes that delay the transition of these kinase molecules from the DFG-out to the DFG-in conformation. This in turn, could increase the sensitivity of these mutants for type II inhibitors, drugs that specifically engage the DFG-out kinase state (Figure 6). This highlights that genomic interrogation alone across fusion-positive cancers may be insufficient to understand the complex steric and conformational changes that govern drug resistance and sensitivity.

It is important to recognize several factors. First, the crystal structures of type II inhibitors have yet to be complexed with TRK kinases to confirm type II binding. We likewise cannot rule out that these drugs bind to TRK via mechanisms beyond simple type II engagement. Second, not all xDFG substitutions are created equal; the size and charge of the substituted amino acid may induce differential phenotypes. For example, we found that Trka G670C-containing models harbored more resistance compared to TrkA G670A-containing models. The larger size of the cysteine (compared to alanine) and the partial negative charge on its sulphur atom may result in more steric hindrance and repulsion of the negatively charged fluoro-containing aromatic groups of the 2nd-generation TRK inhibitors, selitrectinib and repotrectinib. It is thus possible that G→A xDFG substitution-containing cancers could respond initially to therapy, but with less durability compared to cancers harboring other on-target resistance mechanisms.

xDFG mutations were initially identified as acquired resistance mechanisms to 1st-generation type I TRK inhibitors (8,12). Second-generation TKIs were thus designed to maintain activity against these and other more common resistance mutations. A primary design parameter of these small macrocyclic agents was the ability to abrogate steric hindrance resulting from solvent front and gatekeeper residue substitutions. Although second-generation TKIs were effective against many of these resistance mutations, these drugs were still designed as type I inhibitors. As such, these agents were not poised to avoid the penalties of structural shifts into the inactive conformation. Our work thus exposes an occult liability that was not predicted by initial experiments and highlights the inability of 2nd-generation type I TKIs to overcome all forms of on-target resistance.

These observations are potentially applicable to other oncogenic kinases. We demonstrate, for example, that xDFG substitutions not only occur across other kinases known to be involved in recurrent gene fusions but confer sensitivity to type II inhibitors in the context of *ROS1* fusions. It should be noted that adaptive conformational resistance engendered by altering the relative proportion of active or inactive kinase pools can occur in either direction. In BCR-ABL-containing chronic myelogenous leukemia, resistance mutations to 1st-generation TKI therapy with the type II TKI imatinib result in a preferential shift towards an active DFG-in conformation (27), the opposite of what is observed in TRK xDFG resistance. The emergence of mutations that induce conformational shifts has also been reported in EGFR (28), MET (29), KIT (30), RET (31), and ROS1-driven cancers (32).

We show that type II inhibitors overcome xDFG resistance by binding the preferred inactive conformation of these mutant kinases. Although several TKIs are known to engage kinases in an inactive conformation, the vast majority of these agents (e.g. cabozantinib/foretinib) are repurposed multikinase inhibitors that were not intentionally designed to inhibit select targets (33). Therefore, they are characterized by substantial off-target inhibition and consequently a high frequency of side-effects and poor plasma exposures (34). In addition, these agents represent a minority of TKIs that are available in the clinic as most targeted therapies that are either approved (i.e. osimertinib, alectinib, brigatinib, lorlatinib, entrectinib) or in trials are type I inhibitors (35). Rational drug design should thus move towards the development of selective type II kinase inhibitors. While this can be challenging, particularly considering the heterogeneity of mutations that might be amenable to type II kinase inhibition, methods to test the affinity of candidate TKIs against multiple mutation variants have already been reported (36).

In conclusion, our study uncovers a molecular switch induced by xDFG mutations that limits the sensitivity to type I kinase inhibitors. This occurs via the generation of steric hindrance and the induction of conformational changes that favor the inactive DFG-out kinase state. This same switch, in turn, sensitizes these mutant kinases to type II inhibitors that effectively engage the inactive conformation. Ultimately, a combination of selective type I and type II inhibitors might represent the most effective way to address on-target mechanisms of TKI resistance.

METHODS

Patients

Patients were treated with TRK inhibitors as part of prospective IRB-approved research protocols or expanded access protocols. All patients provided written informed consent for genomic sequencing of tumor and cfDNA, and review of medical records for detailed demographic, pathologic, and clinical data and for publication of this information as part of an institutional IRB-approved research protocol (MSKCC; NCT01775072). Research protocols for tumor collection and analysis were approved by the ethical committees of MSKCC.

Compounds

Larotrectinib and selitrectinib were obtained from Loxo Oncology. Repotrectinib was purchased from Selleckchem. Cabozantinib, foretinib, ponatinib, crizotinib and axitinib were purchased from MedChem Express. All drugs were dissolved in DMSO to yield 10mM stocks and stored at −20°C.

Targeted Tumor Sequencing

DNA from formalin-fixed paraffin-embedded tissue and matched germline DNA underwent targeted next-generation sequencing assay using (MSK-IMPACT; (37)). In brief, this assay uses a hybridization-based exon capture designed to capture all protein-coding exons and select introns of oncogenes, tumor-suppressor genes and key members of pathways that may be actionable by targeted therapies. In this study, either 410 or 468 key cancer-associated genes were analyzed. Sequencing data were analyzed as previously described to identify somatic single-nucleotide variants, small insertions and deletions, copy number alterations and structural rearrangements (38). In addition, hotspot alterations were identified using an adaptation of a previously described method (39) applied to a cohort of 24,592 sequenced human cancers (40).

Targeted Plasma Sequencing

Cell-free DNA (cfDNA) was extracted from all plasma samples and sequenced using a custom, ultra-deep coverage next-generation sequencing panel (MSK-ACCESS). The custom assay includes key exons and domains of 129 and introns of 10 genes harboring recurrent breakpoints and uses duplex unique molecular identifiers (UMIs) and dual index barcodes to minimize background sequencing errors and sample-to-sample contamination. Sequencing data were analyzed using a custom bioinformatics pipeline that trims the UMIs, aligns the processed reads to the human genome, collapses PCR replicates into consensus sequences, and re-aligns the error-suppressed consensus reads. Consensus reads with representation from both strands of the original cfDNA duplex were used for de novo variant calling using VarDict (v1.5.1). Mutation calling required at least 1 collapsed read at a known cancer hotspot site or at least 3 collapsed reads at non-hotspot sites. All samples were sequenced to an average depth of approximately 20,000X coverage. Somatic mutations were identified and quantified as variant allele frequencies. Copy number alterations were identified across all samples using a previously described method (38). *NTRK* fusions were identified and quantified using Manta (v1.5.0). All samples were manually reviewed to identify *NTRK* fusions. Variants were called against an unmatched healthy plasma donor to identify any specimen type-related artifacts. Mutations called at silent, intronic, and intergenic loci were removed.

Structure Preparation

The structures of the apo forms of TRKA in its inactive state and of TRKA in its active state were generated using the available crystal structures. A crystal structure of apo TRKA in its inactive state (PDB: 4F0I) is available. The structure of the active form of apo TRKA was generated from the crystal structure of TRKA complexed to a ligand (PDB: 4YNE) by removing the ligand. The 3D structures of the drug molecules larotrectinib, selitrectinib and

repotrectinib were built using Maestro and minimized using the Macromodel module employing the OPLS-2005 force field (41) in Schrodinger 9.0. All the drug molecules were then prepared with Ligprep that generates low energy tautomers and enumerates realistic protonation states at physiological pH. The prepared inhibitors were docked into the ATP binding pocket of the apo forms of TRKA kinase generated above using Glide (42). The docking was carried out under a constraint that a hydrogen bond is formed between the nitrogen atoms from the drug molecules and the backbone amide nitrogen of Met592 in TRKA; this was imposed based on the observation of such a hydrogen bond in the crystal structures of the ROS1 kinase complexed to Ent (Ent is a drug very similar to the drugs considered here; PDB 5KVT) and of TRKA in its active state complexed to a ligand (also very similar to the drugs that are being studied here; PDB 4YNE). A box of size 10 × 10 × 10 Å for molecular docking, centered on the ATP binding site residues of TRKA in its active state was used to define the search space of each docked drug molecule. For the grid generation, the default Glide settings were used. The docked conformation of each ligand was evaluated using the Glide Extra Precision (XP) scoring function. The structural models of the drug molecules foretinib and ponatinib complexed to the inactive states of TRKA were generated using the co-crystal structures of foretinib bound to the inactive state of MET kinase (~39% identity to TRKA; PDB 6SD9) and of ponatinib bound to the inactive state of FGFR4 kinase (~41% identity to TRKA; PDB 4TYI). Both these complex structures were superimposed onto the structure of the inactive state of TRKA and the corresponding complexes of TRKA with foretinib and ponatinib generated. The structural model of cabozantinib complexed to the inactive state of TRKA was generated by modifying foretinib in its complexes with TRKA.

Structural models of the apo forms and complexes of the mutant kinases in both active and inactive forms (G595R, G667C, G667A, G667S, G595R/G667C, G595R/G667A) with the 6 drug molecules (larotrectinib, selitrectinib, repotrectinib, cabozantinib, foretinib, ponatinib) were modelled using the corresponding structures of the wild type kinases using the prime module (the sidechain orientations of the mutations are optimized) from the Schrodinger software. All the structural models were subsequently subjected to molecular dynamics (MD) simulations for further refinement.

MD Simulations

MD simulations were carried out with the pmemd.cuda module of the program Amber18 (43). The partial charges and force field parameters for each drug molecule were generated using the Antechamber module in Amber. All atom versions of the Amber14SB force field (ff14SB) (44) and the general Amber force field (GAFF) (45) were used to model the protein and the drug molecules respectively. The Xleap module of Amber was used to prepare the systems for the MD simulations. All the simulation systems were neutralized with appropriate numbers of counter ions. Each neutralized system was solvated in an octahedral box with TIP3P (46) water molecules, leaving at least 10Å between the solute atoms and the borders of the box. All MD simulations were carried out in explicit solvent at 300K. During the simulations, the long-range electrostatic interactions were treated with the particle mesh Ewald (47) method using a real space cut off distance of 9Å. The Settle (48) algorithm was used to constrain bond vibrations involving hydrogen atoms, which allowed a time step of

2fs during the simulations. Solvent molecules and counter ions were initially relaxed using energy minimization with restraints on the protein and drug atoms. This was followed by unrestrained energy minimization to remove any steric clashes. Subsequently the system was gradually heated from 0 to 300 K using MD simulations with positional restraints (force constant: 50 kcal mol-1 Å-2) on protein and drugs over a period of 0.25 ns allowing water molecules and ions to move freely. During an additional 0.25 ns, the positional restraints were gradually reduced followed by a 2 ns unrestrained MD simulation to equilibrate all the atoms. Finally, production MD simulations were carried out for 250ns in triplicates with conformations stored for every 10ps. Simulation trajectories were visualized using VMD (49) and figures were generated using PyMOL (50). A summary of production of MD simulation details and time of simulations is reported in Supplementary Table S1A–C.

In vitro Kinase Assays

Recombinant kinases were purchased by SignalChem Lifesciences Corporation (Richmond, BC, Canada). *In vitro* kinase assays were performed by Reaction Biology Corp. (Malvern, PA, US). Briefly, compounds (larotrectinib, selitrectinib, cabozantinib, foretinib and ponatinib) were tested in 10-dose IC50 mode with 3-fold serial dilution starting at 2 uM in the presence of 10 uM ATP. Control compound Staurosporine was also tested. Two replicates for each dilution were performed. IC50 was calculated using GraphPad Prism version 8.

Microscale Thermophoresis (MST)

MST experiments were conducted by Reaction Biology Corp. (Malvern, PA, US). Selitrectinib concentrations ranged from 0.015 nM to 1000 nM (16 doses) while cabozantinib and foretinib concentrations ranged from 0.003 nM to 100 nM (16 doses). The concentration of the target (TRKA G667C) was kept constant at 5 nM. Two independent experiments were performed for each drug. Student T-test was used to calculate significant differences in Kds values. $P<0.05$ were considered statistically significant.

Culture of *Bcan-Ntrk1* Mouse Glioma Cells

All mouse p53−/− *Bcan-Ntrk1* glioma cell lines were plated on laminin-coated dishes and cultured in Neurocult Stem Cell Basal Media with Proliferation Supplements (Stem Cell Technologies). The low-density seeding method was performed to isolate a monoclonal cell line harboring desired mutation from electroporated pooled population of mouse p53−/− *Bcan-Ntrk1* glioma cells.

CRISPR-Cas9 Mediated HDR

Cas9-gRNA ribonucleoprotein (RNP) complex and single-stranded oligodeoxynucleotides (ssODNs) were used togenerate Trka mutations in *Bcan-Ntrk1* mouse glioma cells. We used a CRISPR-Cas9 mediated Homology-Directed Repair approach in which cells were nucleofected with the Cas9-gRNA ribonucleoprotein complex together with single-stranded oligodeoxynucleotides (donor template sequences) that harbored the desired substitutions plus additional silent substitution designed to introduce a diagnostic restriction site.

All crRNAs (Alt-R CRISPR-Cas9 crRNA) and ssODNs are synthesized by Integrated DNA Technologies and RNP complex was formed according to the manufacturer's instructions. Sequences of crRNAs and ssODNs are found in Supplementary Table S2A. Briefly, gRNA was assembled by mixing equimolar amounts of crRNA and tracrRNA (Alt-R CRISPR-Cas9 tracrRNA-ATTO-550) and heating to 95°C for 5 min. Cas9 (Alt-R S.p. Cas9 Nuclease V3) and gRNA were incubated for 10 min at room temperature to allow RNP formation. ssODNs and RNP complex were delivered into 1×10^5 mouse p53−/− *Bcan-Ntrk1* glioma cells by 4D-Amaxa Nucleofector System (Lonza) using the Amaxa SF Cell Line Nucleofector X Kit S (Lonza) according to the manufacturer's instructions. Cells were sorted based on ATTO-550 expression 48 h post-nucleofection by the Flow Cytometry Core Facility at MSK.

PCR and RT-PCR for Clone Selection

For PCR analysis of genomic DNA, cells were collected and genomic DNA was extracted by phenol:chloroform:isoamyl alcohol (Invitrogen). For RT-PCR, total RNA was isolated from cells using Trizol reagent (Invitrogen) and cDNA was generated using SuperScript III First-Strand Synthesis System (Invitrogen). The primers used in the various PCR reactions are provided in Supplementary Table S2B.

CRISPR Sequencing

A ~ 200 bp region encompassing the modified locus targeted by CRISPR was PCR amplified from isolated genomic DNA and amplicon was gel purified (NEB). Each amplicon was sequenced to 75,000–100,000 reads sequencing. Reads were analyzed using CRISPResso by the MSKCC Integrated Genomics Operation.

Drug Screenings

Cell-Titer Glo-based assay: *LMNA-NTRK1*, TRKA G595R and *LMNA-NTRK1*, TRKA G595R/G667C primary CRC cell lines or the isogenic mouse glioma cell lines were seeded in 96 well-plates (6,000 per well). The following day larotrectinib, selitrectinib, repotrectinib, cabozantinib, foretinib, ponatinib, crizotinib or axitinib (1:2 dilutions starting with a maximum concentration of 1000nM) was added. Cell-Titer Glo reagent was added 72 hours later and absorbance was read at 490nm according to the manufacturer protocol. Data are presented as % cell viability (mean±SD) normalized to the DMSO treated cells considered 100% viable.

Antibodies and Western Blots

Cells were seeded in 6 Well Plates (500000) per condition in full medium. The day after, cells were treated with 50nM of each compound for 30 minutes. Total protein lysates were extracted using RIPA buffer and quantified using BCA according to the manufacturer's protocol. Lysates were separated using SDS-PAGE gels according to standard methods. Membranes were probed using the following antibodies: pan Trk clone A7H6R (92991S Cell Signaling Technology), phospho TrkA (Y674/675) clone C50F3 (4621S Cell Signaling Technology), phospho MEK1/2 (S217/221) clone 41G9 (9154S Cell Signaling Technology), total MEK1/2 (9122L Cell Signaling Technology), phospho p44/42 MAPK (Erk1/2; T202/

Y204) clone D13.14.4E (4370S Cell Signaling Technology), total ERK1/2 (9102S Cell Signaling Technology), Phospho-Met (Tyr1234/1235) (3129S, clone 3D7 Cell Signaling Technology), total MET (8198S, clone D1C2 Cell Signaling Technology), V5 (A00623–100 GeneScripts), phospho Tyrosine (4G10® Platinum, Anti-Phosphotyrosine 05–1050X Millipore), total ROS1 (3266S, clone 69D6, Cell Signaling Technology), phospho ROS1 (Tyr2274) (3078S Cell Signaling Technology) and β-actin clone 13E5 (4970S Cell Signaling Technology).

Intracranial Injection

Four-to six months-old female NSG female mice were anaesthetized with ketamine/xylazine and treated with a pre-operative dose of buprenorphine prior to craniotomy. 500,000 cells of mouse *Bcan-Ntrk1* glioma cells harboring the Trka G670C substitution were delivered per animal via stereotactic intracranial injection targeting the neurogenic region of the right lateral ventricle. One week later, brain magnetic resonance imaging (MRI) was performed using a Bruker 4.7T Biospec scanner by the Animal Imaging Core Facility at Memorial Sloan Kettering Cancer Center. Images were visualized with the online miniPACS software. Mice were then randomized based on tumor size (calculated using ImageJ software) in vehicle (n=3) and cabozantinib (n=4) groups. Animals were treated with vehicle or cabozantinib daily (100mg/ml) via oral gavage. At day 7 of treatment, a second MRI was performed using the same scanner. Tumor size was quantified in both groups and data were then analysed using GraphPad 8.1.2. Treatments were continued until mice' sacrifice to obtain survival curves. Mouse experiments were approved by MSKCC's Institutional Animal Care and Use Committee.

Patient-derived Primary Cell Lines

The entrectinib-resistant *LMNA-NTRK1*, TRKA G595R CRC cell line was obtained from Dr. Alberto Bardelli (Candiolo Cancer Institute, FPO, IRCCS, Turin, Italy). The *LMNA-NTRK1*, TRKA G595R/G667C cell line was established following chronic exposure of the *LMNA-NTRK1*, TRKA G595R to increasing concentrations of repotrectinib (ranging from 1 to 500nM) for five months. Cell lines were plated on petri dishes and cultured in DMEM/F12 + 10% FBS and 1% antibiotics.

Xenografts and PDX Studies

Xenografts derived from the *LMNA-NTRK1*, TRKA G595R/TRKA G667C colorectal cancer primary cell line were generated by injecting 5 million of cells into the flank of six-weeks-old NSG female mice. When tumors reached 100 mm^3 in size, mice were randomized and dosed orally with vehicle, repotrectinib (100mg/kg daily 5 days per week) or cabozantinib (100mg/Kg daily 5 days per week). PDXs derived from Patient 1 were randomized and dosed orally with vehicle, selitrectinib (100mg/kg BID 5 days per week) or cabozantinib (100mg/Kg daily 5 days per week). PDXs derived from Patient 3 were randomized and dosed orally with vehicle, selitrectinib (100mg/kg BID 5 days per week), repotrectinib (100mg/kg daily 5 days per week) or cabozantinib (100mg/Kg daily 5 days per week). Tumors were measured twice weekly using calipers, and tumor volume was calculated using the formula length × $width^2$ × 0.52. Body weight was also assessed twice weekly. Mice were cared for in accordance with guidelines approved by the MSK

Institutional Animal Care and Use Committee and Research Animal Resource Center. Six to eight mice per group were included in each experiment.

Supplementary Material

Refer to Web version on PubMed Central for supplementary material.

Acknowledgments

FUNDINGS

This study was funded by the National Cancer Institute (NCI) under the MSK Cancer Center Support Grant/Core Grant (P30 CA008748) and the R01CA226864 (to MS and AD). This work was also funded by the Cycle for Survival (to AD), Nonna's Garden Foundation (AD, ASM, DH, MS), NIH T32 CA009207, and ASCO Young Investigator Award (A.M.S). Work by J.E.L. and A.V. was funded by the Geoffrey Beene Cancer Research Foundation, the STARR Foundation, and by the Pershing Square Cancer Research Foundation. E.C. is a recipient of an MSK society scholar prize and of a NIH sponsored Translational Research in Oncology Training (TROT) fellowship (5 T32 CA160001-08). We thank A*STAR (IAF-PP grant H18/01/a0/015) and the National Supercomputing Centre (NSCC), Singapore for support. The work was also supported by The United State—Israel Binational Science Foundation (BSF, 2017323) (to M.E and M.S). Work of Y.L. and U.R. was funded by the R01CA181746 (to UR). The research leading to these results has received funding from FONDAZIONE AIRC under 5 per Mille 2018 - ID. 21091 program – P.I. Bardelli Alberto; AIRC IG 2018 - ID. 21923 project - PI Bardelli Alberto; Fondazione Piemontese per la Ricerca sul Cancro-ONLUS 5 per mille 2014 e 2015 Ministero della Salute (A.B.); AIRC under MFAG 2017 -ID 20236 project -P.I. Arena Sabrina.

CONFLICT OF INTERESTS STATEMENT

M.S. has received research funds from Puma Biotechnology, AstraZeneca, Daiichi Sankyo, Immunomedics, Targimmune and Menarini Ricerche. He is in the scientific advisory board (SAB) of Menarini Ricerche and Bioscience Institute and is a cofounder of Medendi.org.

A.D. has received honoraria from Ignyta/Genentech/Roche, Loxo/Bayer/Lilly, Takeda/Ariad/Millenium, TP Therapeutics, AstraZeneca, Pfizer, Blueprint Medicines, Helsinn, Beigene, BergenBio, Hengrui Therapeutics, Exelixis, Tyra Biosciences, Verastem, MORE Health and Abbvie. A.D. also received research funds from Pfizer, Exelixis, GlaxoSmithKlein, Teva, Taiho, PharmaMar and Foundation Medicine and royalties from Wolters Kluwer. Food/beverage was provided to A.D. by Merck, PUMA and MERUS. A.D. received CME honoraria from Medscape, OncLive, PeerVoice, Physicians Education Resources, Targeted Oncology, Research to Practice and Oncology. D.M.H. had consulting or advisory roles for Chugai Pharma, CytomX Therapeutics, Boehringer Ingelheim, AstraZeneca, Pfizer, Bayer Pharmaceuticals and Genentech / Roche. D.M.H. also received research funds from Loxo Oncology, PUMA Biotechnology, AstraZeneca and Bayer Pharmaceuticals and travel expenses from Genentech and Chugai Pharma. SK and CSV are founder directors of SiNOPSEE Therapeutics and Aplomex. C.S.V has been the recipient of research grants (not related to this work) from Ipsen Pharmaceuticals, MSD International and Proctor & Gamble, administered through A*STAR, Singapore.

REFERENCES

1. Recondo G, Facchinetti F, Olaussen KA, Besse B, Friboulet L. Making the first move in EGFR-driven or ALK-driven NSCLC: first-generation or next-generation TKI? Nat Rev Clin Oncol 2018;15(11):694–708 doi 10.1038/s41571-018-0081-4. [PubMed: 30108370]
2. Lin JJ, Riely GJ, Shaw AT. Targeting ALK: Precision Medicine Takes on Drug Resistance. Cancer Discov 2017;7(2):137–55 doi 10.1158/2159-8290.CD-16-1123. [PubMed: 28122866]
3. Lin JJ, Shaw AT. Recent Advances in Targeting ROS1 in Lung Cancer. J Thorac Oncol 2017;12(11):1611–25 doi 10.1016/j.jtho.2017.08.002. [PubMed: 28818606]
4. Schram AM, Chang MT, Jonsson P, Drilon A. Fusions in solid tumours: diagnostic strategies, targeted therapy, and acquired resistance. Nat Rev Clin Oncol 2017;14(12):735–48 doi 10.1038/nrclinonc.2017.127. [PubMed: 28857077]
5. Vasan N, Baselga J, Hyman DM. A view on drug resistance in cancer. Nature 2019;575(7782):299–309 doi 10.1038/s41586-019-1730-1. [PubMed: 31723286]

6. Cocco E, Schram AM, Kulick A, Misale S, Won HH, Yaeger R, et al. Resistance to TRK inhibition mediated by convergent MAPK pathway activation. Nat Med 2019;25(9):1422–7 doi 10.1038/s41591-019-0542-z. [PubMed: 31406350]
7. Cocco E, Scaltriti M, Drilon A. NTRK fusion-positive cancers and TRK inhibitor therapy. Nat Rev Clin Oncol 2018;15(12):731–47 doi 10.1038/s41571-018-0113-0. [PubMed: 30333516]
8. Drilon A, Laetsch TW, Kummar S, DuBois SG, Lassen UN, Demetri GD, et al. Efficacy of Larotrectinib in TRK Fusion-Positive Cancers in Adults and Children. N Engl J Med 2018;378(8):731–9 doi 10.1056/NEJMoa1714448. [PubMed: 29466156]
9. Drilon A, Siena S, Ou SI, Patel M, Ahn MJ, Lee J, et al. Safety and Antitumor Activity of the Multitargeted Pan-TRK, ROS1, and ALK Inhibitor Entrectinib: Combined Results from Two Phase I Trials (ALKA-372–001 and STARTRK-1). Cancer Discov 2017;7(4):400–9 doi 10.1158/2159-8290.CD-16-1237. [PubMed: 28183697]
10. Demetri GD, Paz-Ares L, Farago AF, Liu SV, Chawla SP, Tosi D, et al. LBA17Efficacy and safety of entrectinib in patients with NTRK fusion-positive (NTRK-fp) Tumors: Pooled analysis of STARTRK-2, STARTRK-1 and ALKA-372–001. Annals of Oncology 2018;29(suppl_8) doi 10.1093/annonc/mdy424.017.
11. Drilon A, Li G, Dogan S, Gounder M, Shen R, Arcila M, et al. What hides behind the MASC: clinical response and acquired resistance to entrectinib after ETV6-NTRK3 identification in a mammary analogue secretory carcinoma (MASC). Ann Oncol 2016;27(5):920–6 doi 10.1093/annonc/mdw042. [PubMed: 26884591]
12. Russo M, Misale S, Wei G, Siravegna G, Crisafulli G, Lazzari L, et al. Acquired Resistance to the TRK Inhibitor Entrectinib in Colorectal Cancer. Cancer Discov 2016;6(1):36–44 doi 10.1158/2159-8290.CD-15-0940. [PubMed: 26546295]
13. Drilon A, Nagasubramanian R, Blake JF, Ku N, Tuch BB, Ebata K, et al. A Next-Generation TRK Kinase Inhibitor Overcomes Acquired Resistance to Prior TRK Kinase Inhibition in Patients with TRK Fusion-Positive Solid Tumors. Cancer Discov 2017;7(9):963–72 doi 10.1158/2159-8290.CD-17-0507. [PubMed: 28578312]
14. Drilon A, Ou SI, Cho BC, Kim DW, Lee J, Lin JJ, et al. Repotrectinib (TPX-0005) Is a Next-Generation ROS1/TRK/ALK Inhibitor That Potently Inhibits ROS1/TRK/ALK Solvent- Front Mutations. Cancer Discov 2018;8(10):1227–36 doi 10.1158/2159-8290.CD-18-0484. [PubMed: 30093503]
15. Modi V, Dunbrack RL, Jr. Defining a new nomenclature for the structures of active and inactive kinases. Proc Natl Acad Sci U S A 2019;116(14):6818–27 doi 10.1073/pnas.1814279116. [PubMed: 30867294]
16. Zhang J, Yang PL, Gray NS. Targeting cancer with small molecule kinase inhibitors. Nat Rev Cancer 2009;9(1):28–39 doi 10.1038/nrc2559. [PubMed: 19104514]
17. Vijayan RS, He P, Modi V, Duong-Ly KC, Ma H, Peterson JR, et al. Conformational analysis of the DFG-out kinase motif and biochemical profiling of structurally validated type II inhibitors. J Med Chem 2015;58(1):466–79 doi 10.1021/jm501603h. [PubMed: 25478866]
18. Bagal SK, Andrews M, Bechle BM, Bian J, Bilsland J, Blakemore DC, et al. Discovery of Potent, Selective, and Peripherally Restricted Pan-Trk Kinase Inhibitors for the Treatment of Pain. J Med Chem 2018;61(15):6779–800 doi 10.1021/acs.jmedchem.8b00633. [PubMed: 29944371]
19. Fuse MJ, Okada K, Oh-Hara T, Ogura H, Fujita N, Katayama R. Mechanisms of Resistance to NTRK Inhibitors and Therapeutic Strategies in NTRK1-Rearranged Cancers. Mol Cancer Ther 2017;16(10):2130–43 doi 10.1158/1535-7163.MCT-16-0909. [PubMed: 28751539]
20. Konicek BW, Capen AR, Credille KM, Ebert PJ, Falcon BL, Heady GL, et al. Merestinib (LY2801653) inhibits neurotrophic receptor kinase (NTRK) and suppresses growth of NTRK fusion bearing tumors. Oncotarget 2018;9(17):13796–806 doi 10.18632/oncotarget.24488. [PubMed: 29568395]
21. Shen B, Wu F, Ye J, Liang R, Wang R, Yu R, et al. Crizotinib-resistant MET mutations in gastric cancer patients are sensitive to type II tyrosine kinase inhibitors. Future Oncol 2019;15(22):2585–93 doi 10.2217/fon-2019-0140. [PubMed: 31339066]

22. Smith CC, Lin K, Stecula A, Sali A, Shah NP. FLT3 D835 mutations confer differential resistance to type II FLT3 inhibitors. Leukemia 2015;29(12):2390–2 doi 10.1038/leu.2015.165. [PubMed: 26108694]

23. Hari SB, Merritt EA, Maly DJ. Sequence determinants of a specific inactive protein kinase conformation. Chem Biol 2013;20(6):806–15 doi 10.1016/j.chembiol.2013.05.005. [PubMed: 23790491]

24. Drilon A, Jenkins C, Iyer S, Schoenfeld A, Keddy C, Davare MA. ROS1-dependent cancers - biology, diagnostics and therapeutics. Nat Rev Clin Oncol 2020; in press doi 10.1038/s41571-020-0408-9.

25. Cook PJ, Thomas R, Kannan R, de Leon ES, Drilon A, Rosenblum MK, et al. Somatic chromosomal engineering identifies BCAN-NTRK1 as a potent glioma driver and therapeutic target. Nat Commun 2017;8:15987 doi 10.1038/ncomms15987. [PubMed: 28695888]

26. Ciccarese C, Iacovelli R, Mosillo C, Tortora G. Exceptional Response to Cabozantinib of Rapidly Evolving Brain Metastases of Renal Cell Carcinoma: A Case Report and Review of the Literature. Clin Genitourin Cancer 2018;16(5):e1069–e71 doi 10.1016/j.clgc.2018.06.005. [PubMed: 30005936]

27. Lovera S, Morando M, Pucheta-Martinez E, Martinez-Torrecuadrada JL, Saladino G, Gervasio FL. Towards a Molecular Understanding of the Link between Imatinib Resistance and Kinase Conformational Dynamics. PLoS Comput Biol 2015;11(11):e1004578 doi 10.1371/journal.pcbi.1004578. [PubMed: 26606374]

28. Brown BP, Zhang YK, Westover D, Yan Y, Qiao H, Huang V, et al. On-target Resistance to the Mutant-Selective EGFR Inhibitor Osimertinib Can Develop in an Allele-Specific Manner Dependent on the Original EGFR-Activating Mutation. Clin Cancer Res 2019;25(11):3341–51 doi 10.1158/1078-0432.CCR-18-3829. [PubMed: 30796031]

29. Bahcall M, Sim T, Paweletz CP, Patel JD, Alden RS, Kuang Y, et al. Acquired METD1228V Mutation and Resistance to MET Inhibition in Lung Cancer. Cancer Discov 2016;6(12):1334–41 doi 10.1158/2159-8290.CD-16-0686. [PubMed: 27694386]

30. Laine E, Auclair C, Tchertanov L. Allosteric communication across the native and mutated KIT receptor tyrosine kinase. PLoS Comput Biol 2012;8(8):e1002661 doi 10.1371/journal.pcbi.1002661. [PubMed: 22927810]

31. Nakaoku T, Kohno T, Araki M, Niho S, Chauhan R, Knowles PP, et al. A secondary RET mutation in the activation loop conferring resistance to vandetanib. Nat Commun 2018;9(1):625 doi 10.1038/s41467-018-02994-7. [PubMed: 29434222]

32. Drilon A, Somwar R, Wagner JP, Vellore NA, Eide CA, Zabriskie MS, et al. A Novel Crizotinib-Resistant Solvent-Front Mutation Responsive to Cabozantinib Therapy in a Patient with ROS1-Rearranged Lung Cancer. Clin Cancer Res 2016;22(10):2351–8 doi 10.1158/1078-0432.CCR-15-2013. [PubMed: 26673800]

33. Oliveres H, Pineda E, Maurel J. MET inhibitors in cancer: pitfalls and challenges. Expert Opin Investig Drugs 2020;29(1):73–85 doi 10.1080/13543784.2020.1699532.

34. Sumi NJ, Ctortecka C, Hu Q, Bryant AT, Fang B, Remsing Rix LL, et al. Divergent Polypharmacology-Driven Cellular Activity of Structurally Similar Multi-Kinase Inhibitors through Cumulative Effects on Individual Targets. Cell Chem Biol 2019;26(9):1240–52 e11 doi 10.1016/j.chembiol.2019.06.003. [PubMed: 31257184]

35. Ferguson FM, Gray NS. Kinase inhibitors: the road ahead. Nat Rev Drug Discov 2018;17(5):353–77 doi 10.1038/nrd.2018.21. [PubMed: 29545548]

36. Ikemura S, Yasuda H, Matsumoto S, Kamada M, Hamamoto J, Masuzawa K, et al. Molecular dynamics simulation-guided drug sensitivity prediction for lung cancer with rare EGFR mutations. Proc Natl Acad Sci U S A 2019;116(20):10025–30 doi 10.1073/pnas.1819430116. [PubMed: 31043566]

37. Zehir A, Benayed R, Shah RH, Syed A, Middha S, Kim HR, et al. Mutational landscape of metastatic cancer revealed from prospective clinical sequencing of 10,000 patients. Nat Med 2017;23(6):703–13 doi 10.1038/nm.4333. [PubMed: 28481359]

38. Cheng DT, Mitchell TN, Zehir A, Shah RH, Benayed R, Syed A, et al. Memorial Sloan Kettering-Integrated Mutation Profiling of Actionable Cancer Targets (MSK-IMPACT): A Hybridization

Capture-Based Next-Generation Sequencing Clinical Assay for Solid Tumor Molecular Oncology. J Mol Diagn 2015;17(3):251–64 doi 10.1016/j.jmoldx.2014.12.006. [PubMed: 25801821]

39. Chang MT, Asthana S, Gao SP, Lee BH, Chapman JS, Kandoth C, et al. Identifying recurrent mutations in cancer reveals widespread lineage diversity and mutational specificity. Nat Biotechnol 2016;34(2):155–63 doi 10.1038/nbt.3391. [PubMed: 26619011]
40. Chang MT, Bhattarai TS, Schram AM, Bielski CM, Donoghue MTA, Jonsson P, et al. Accelerating Discovery of Functional Mutant Alleles in Cancer. Cancer Discov 2018;8(2):174–83 doi 10.1158/2159-8290.CD-17-0321. [PubMed: 29247016]
41. Kaminski GA, Friesner RA, Tirado-Rives J, Jorgensen WL. Evaluation and Reparametrization of the OPLS-AA Force Field for Proteins via Comparison with Accurate Quantum Chemical Calculations on Peptides. The Journal of Physical Chemistry B 2001;105(28):6474–87 doi 10.1021/jp003919d.
42. Friesner RA, Banks JL, Murphy RB, Halgren TA, Klicic JJ, Mainz DT, et al. Glide: a new approach for rapid, accurate docking and scoring. 1. Method and assessment of docking accuracy. J Med Chem 2004;47(7):1739–49 doi 10.1021/jm0306430. [PubMed: 15027865]
43. Case DA, Ben-Shalom IY, Brozell SR, Cerutti DS, Cheatham TE, Cruzeiro VWD, et al. AMBER 2018. University of California, San Francisco 2018.
44. Maier JA, Martinez C, Kasavajhala K, Wickstrom L, Hauser KE, Simmerling C. ff14SB: Improving the Accuracy of Protein Side Chain and Backbone Parameters from ff99SB. J Chem Theory Comput 2015;11(8):3696–713 doi 10.1021/acs.jctc.5b00255. [PubMed: 26574453]
45. Wang J, Wolf RM, Caldwell JW, Kollman PA, Case DA. Development and testing of a general amber force field. J Comput Chem 2004;25(9):1157–74 doi 10.1002/jcc.20035. [PubMed: 15116359]
46. Jorgensen WL, Chandrasekhar J, Madura JD, Impey RW, Klein ML. Comparison of Simple Potential Functions for Simulating Liquid Water. J Chem Phys 1983;79(2):926–35 doi Doi 10.1063/1.445869.
47. 3rd Current Topics in Gastroenterology Symposium. Sandpiper, Florida, October 31-November 2, 1993. Proceedings. Scand J Gastroenterol Suppl 1995;208:1–148. [PubMed: 7777788]
48. Miyamoto S, Kollman PA. Settle: An analytical version of the SHAKE and RATTLE algorithm for rigid water models. Journal of Computational Chemistry 1992;13(8):952–62 doi 10.1002/jcc.540130805.
49. Humphrey W, Dalke A, Schulten K. VMD: visual molecular dynamics. J Mol Graph 1996;14(1):33–8, 27-8 doi 10.1016/0263-7855(96)00018-5. [PubMed: 8744570]
50. DeLano WL. The PyMOL molecular graphics system. . De Lano Scientific, San Carlos 2002.

SIGNIFICANCE

In TRK fusion-positive cancers, TRK xDFG substitutions represent a shared liability for type I TRK inhibitors. In contrast, they represent a potential biomarker of type II TRK inhibitor activity. As all currently available type II agents are multikinase inhibitors, rational drug design should focus on selective type II inhibitors creation.

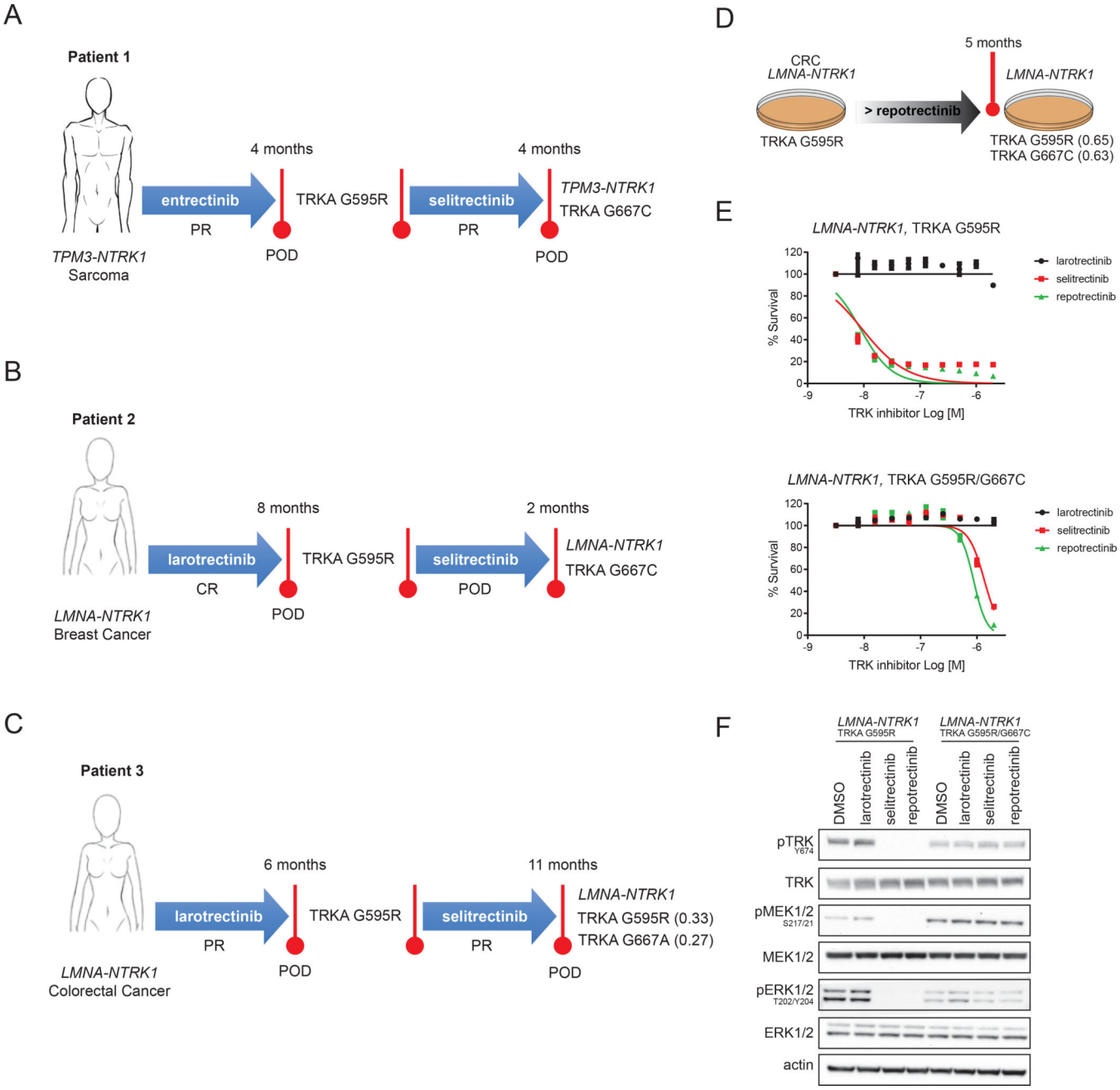

Figure 1. TRKA G667 Mutations Mediate Resistance to Second-generation TRK inhibitors in Patients and Preclinical Models

Schematic showing the emergence of TRKA G667 mutations at progression on the 2nd-generation TRK inhibitor selitrectinib in a *TPM3-NTRK1*, TRKA G595R mutated sarcoma patient (Patient 1; A), a *LMNA-NTRK1*, TRKA G595R mutated breast cancer patient (Patient 2; B) and a *LMNA-NTRK1*, TRKA G595R mutated colorectal cancer patient (CRC, Patient 3; C). Note that while in both Patient 1 and Patient 2 the TRKA G595R was not detected in the selitrectinib-resistant sample, this mutation persisted in the selitrectinib-resistant tumor of Patient 3 (the allele frequencies of the TRKA G595R and the TRKA G667A mutations are indicated in parenthesis). PR: Partial Response; POD: Progression of

Disease. All three patients were treated with a 1st-generation TRK inhibitor (entrectinib for Patient 1 and larotrectinib for Patient 2 and 3) prior receiving selitrectinib and achieved a partial or complete response. At progression, sequencing of the resistant tumors revealed the presence of a TRKA G595R mutations in all three cases (A-C). (D) Schematic showing the emergence of a TRKA G667C mutation in a *LMNA-NTRK1*, TRKA G595R mutated primary CRC cell line that became resistant to the 2nd-generation TRK inhibitor repotrectinb following chronic drug exposure. Cell-Titer-Glo-based proliferation assays (E) and Western blot analyses (F) confirming that the *LMNA-NTRK1*, TRKA G595R/G667C double mutant CRC cell line is resistant to both selitrectinib and repotrectinib.

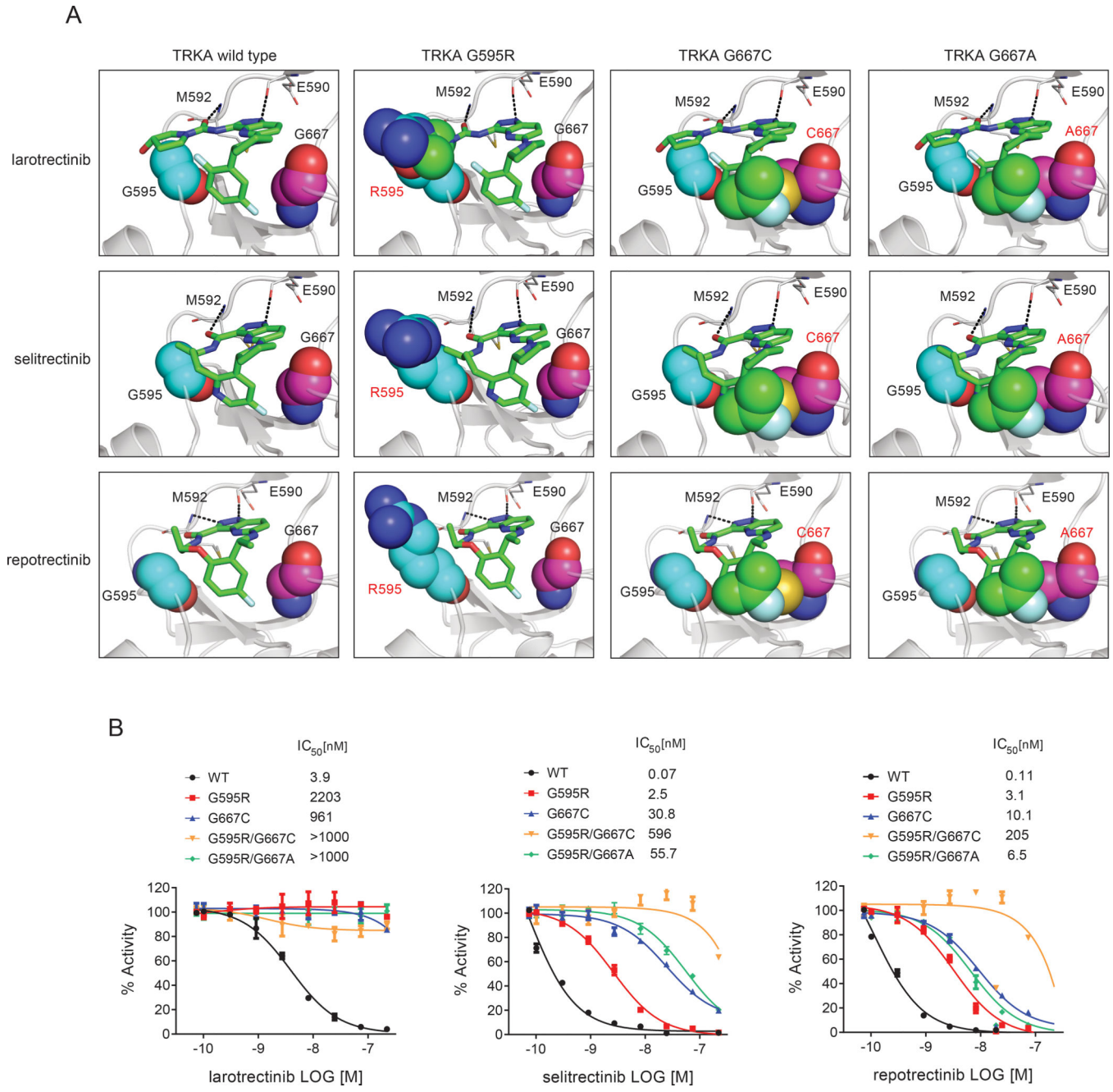

Figure 2. TRKA G667 Substitutions Generate Steric Hindrance that Compromises Selitrectinib and Repotrectinib Binding

(A) Representative models from Molecular Dynamics (MD) simulations showing larotrectinib, selitrectinib and repotrectinib in complex with TRKA wild type, TRKA G595R, TRKA G667C and TRKA G667A mutants. Bound drugs (green sticks) and kinase residues 595 and 667 (colored spheres) are displayed. Chemical groups of larotrectinib, selitrectinib and repotrectinib that clash with mutant TRKA kinases are depicted as spheres for visualization purposes. (B) Radiometric *in vitro* kinase assays showing the kinase activity of TRKA wild type (WT), TRKA G595R and TRKA G667C single mutants and

TRKA G595R/G667C and TRKA G595R/G667A double mutants treated with increasing concentrations of larotrectinib, selitrectinib and repotrectinib. Kinase activities are presented as % (mean±SD) considering an activity of 100% in the untreated kinases set as controls. IC_{50} calculated for each drug against the different kinases are indicated. Experiments were run in duplicates.

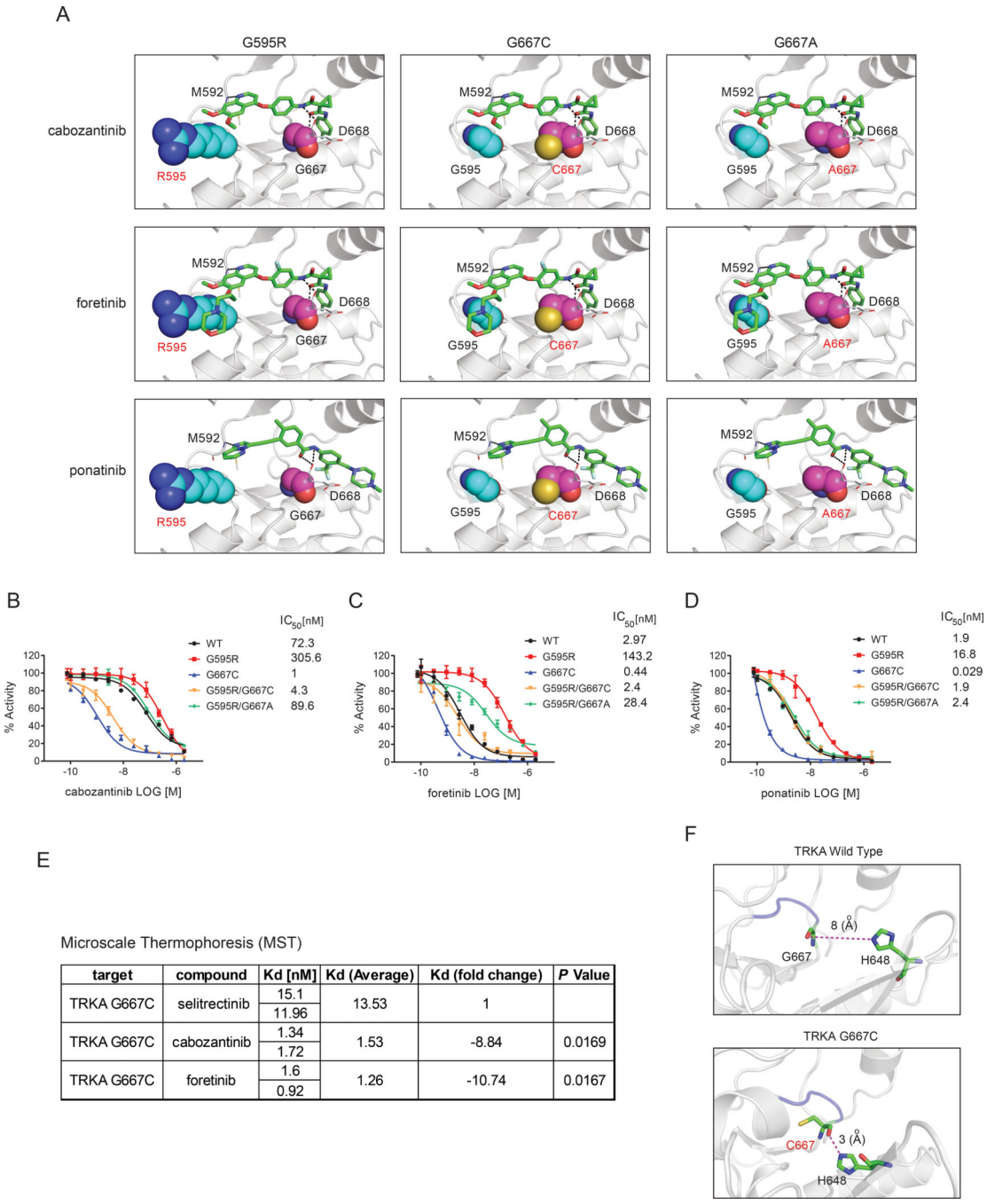

Microscale Thermophoresis (MST)

target	compound	Kd [nM]	Kd (Average)	Kd (fold change)	*P* Value
TRKA G667C	selitrectinib	15.1 11.96	13.53	1	
TRKA G667C	cabozantinib	1.34 1.72	1.53	-8.84	0.0169
TRKA G667C	foretinib	1.6 0.92	1.26	-10.74	0.0167

Figure 3. Type II TRK Inhibitors Preferentially Bind to and Inhibit the Activity of TRKA xDFG Mutants

(A) Representative models representing the most sampled conformations based on clustering the conformations generated during the Molecular Dynamics (MD) simulations showing cabozantinib, foretinib and ponatinib in complex with TRKA G595R, TRKA G667C and TRKA G667A mutants; clustering was carried out using the K-clust algorithm based on the RMSD of the protein structures and only one major cluster (representing >90% of the conformations sampled) was seen for each complex. Bound drugs (green sticks) and kinase residues 595 and 667 (colored spheres) are displayed. (B-D) Radiometric *in vitro* kinase

assays showing the kinase activity of TRKA WT, TRKA G595R and TRKA G667C single mutants and TRKA G595R/G667C and TRKA G595R/G667A double mutants treated with increasing concentrations of cabozantinib (B), foretinib (C) and ponatinib (D). Kinase activities are presented as % (mean±SD) considering an activity of 100% in the untreated kinases set as controls. IC_{50} calculated for each drug against the different kinases are indicated. Experiments were run in duplicates. (E) Determination of the binding affinity (Kd) of the type I inhibitor selitrectinib and the type II inhibitors cabozantinib and foretinib for the TRKA G667C mutant kinase in Microscale Thermophoresis (MST) assays. Kd fold changes are indicated (Average Kd of selitrectinib has been set as reference). Experiments were run in duplicates and P value was calculated using Student T-Test. (F) Representative models representing the most sampled conformations based on clustering the conformations generated during the Molecular Dynamics simulations showing the interactions between the Gly667/Cys667 - His648 in the inactive forms of TRKA WT (upper panel) and TRKA G667C (lower panel) kinases; clustering was carried out using the K-clust algorithm based on the RMSD of the protein structures and only one major cluster (representing >90% of the conformations sampled) was seen for each complex. Kinases are shown as cartoons (grey), the residues Gly/Cys667 and His648 are highlighted (green sticks) and the interactions (H-bound) between residues are shown as dashed lines (magenta).

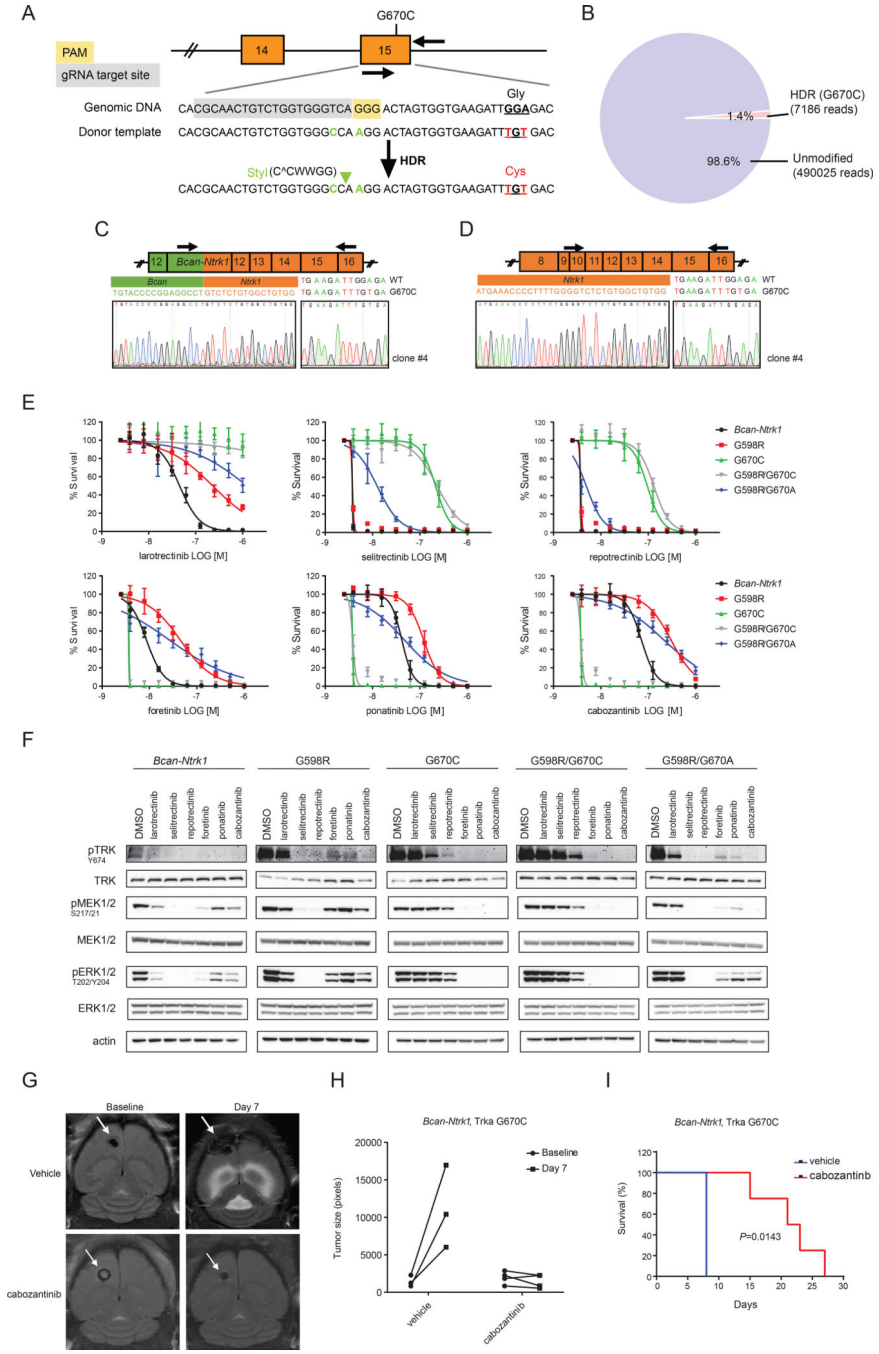

Figure 4. TRKA xDFG Mutated *Bcan-Ntrk1* Mouse Glioma Cells Respond to Type II TRK Inhibitors

(A-D) Strategy for the generation of knock-in isogenic *Bcan-Ntrk1* glioma cells harboring the Trka G670C mutation is described. Sequences of gRNA and single strand donor template are shown. Cys670 (TGT) substitution is indicated (red). Silent mutations (green) in the point accepted mutation (PAM, in yellow) and gRNA seed sequence creating a new restriction site (green arrow head) to facilitate clones' selection are also highlighted. CRISPR-Cas9 induced HDR event counts for G670C mutation in a pooled cell population was determined after FACS-sorting by CRISPR-sequencing (B). RT-PCR using primers

(black arrows) designed to detect the *Bcan-Ntrk1* fusion transcript (C) or non-fused WT *Ntrk1* transcript (D) was performed on total RNA. Sanger sequencing results of RT-PCR products are shown. Cell-Titer-Glo-based assays (E) and Western blot analyses (a representative experiment of a total of three independent replicates, F) performed on the *Bcan-Ntrk1* WT and mutant clones showing the effect of type I (i.e., larotrectinib, selitrectinib and repotrectinib) and type II (i.e., cabozantinib, foretinib and ponatinib) TRK inhibitors on cell proliferation and TrkA-mediated downstream signaling. Proliferation assays are plotted as % survival normalized on control, untreated cells. Data of three independent experiments are plotted as mean±SD (E). (G) Representative Magnetic Resonance Imaging (MRI) scans of orthotopic mouse gliomas at baseline or 7 days after daily treatment with vehicle (upper panel) or cabozantinib (100mg/Kg; lower panel). (H) Quantification of tumor size in vehicle-treated control mice (n=3) and in cabozantinib-treated mice (n=4) at baseline and after 7 days of daily treatment. Volume was calculated using ImageJ (in pixels). Each mouse was independently plotted. (I) Survival curves of vehicle and cabozantinib-treated mice. Note: mice received daily treatment until sacrifice. Mantel-Cox test was used to calculate significant differences between the two groups. A P value <0.05 was considered statistically significant.

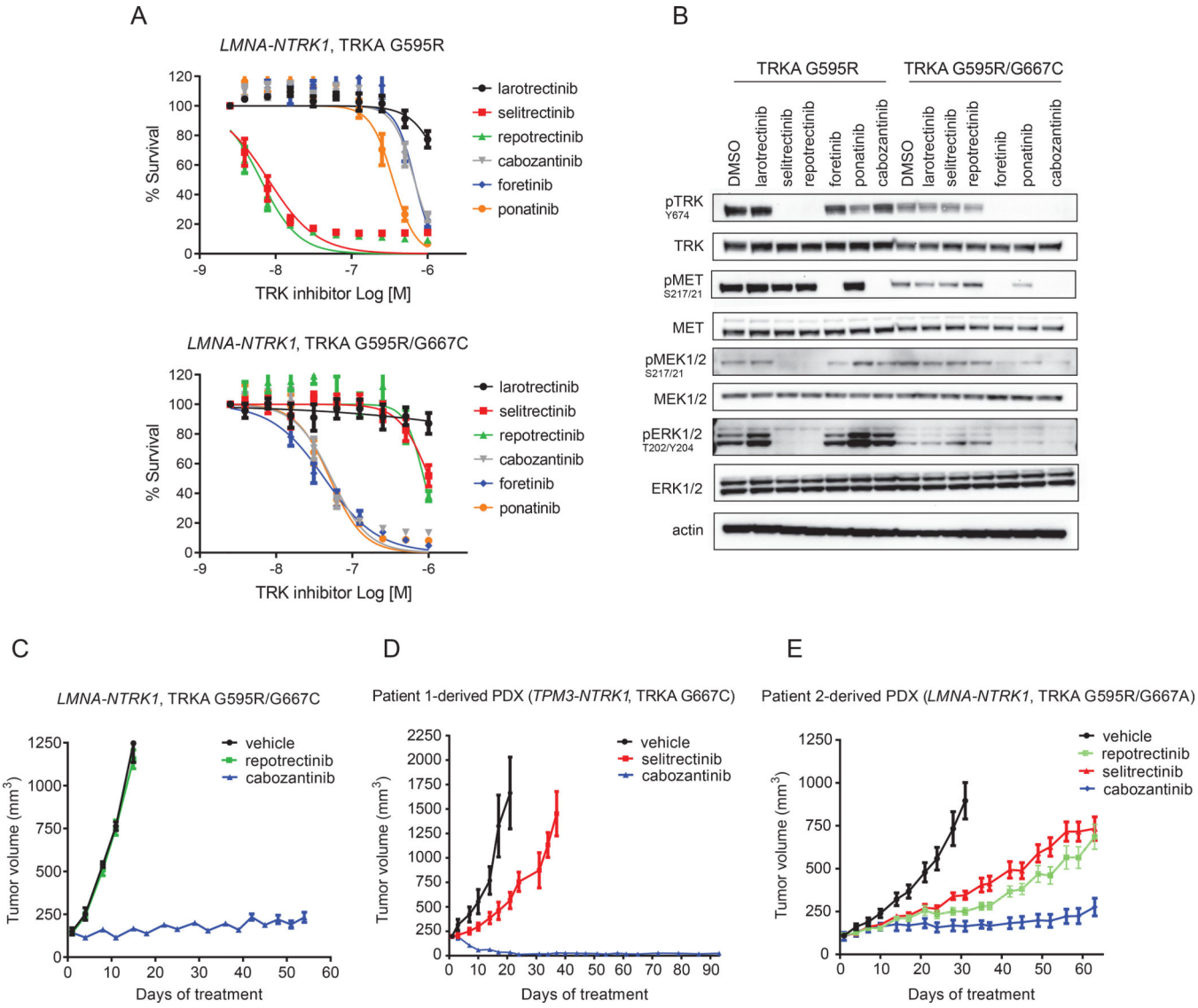

Figure 5. Type II Drugs Overcome Resistance to Second-generation TRK Inhibitors in Patient-derived Models

Cell-Titer-Glo-based assays (A) and Western blot analyses (a representative experiment of a total of three independent replicates, B) performed on the *LMNA-NTRK1*, TRKA G595R and the *LMNA-NTRK1*, TRKA G595R/G667C double mutant primary colorectal cancer (CRC) cell lines showing the effect of type I (i.e., larotrectinib, selitrectinib and repotrectinib) and type II (i.e., cabozantinib, foretinib and ponatinib) TRK inhibitors on cell proliferation and TrkA-mediated downstream signaling. Proliferation assays are plotted as % survival normalized on control, untreated cells. Data of three independent experiments are plotted as mean±SD (A). *In vivo* efficacy of cabozantinib in xenografts established from the repotrectinib-resistant *LMNA-NTRK1*, TRKA G595R/G667C double mutant primary CRC (C) and in PDXs established from the selitrectinib-resistant tumor of Patient 1 (*TPM3-NTRK1*, TRKA G667C sarcoma; D) and Patient 3 (*LMNA-NTRK1,* TRKA G595R/G667A CRC; E).

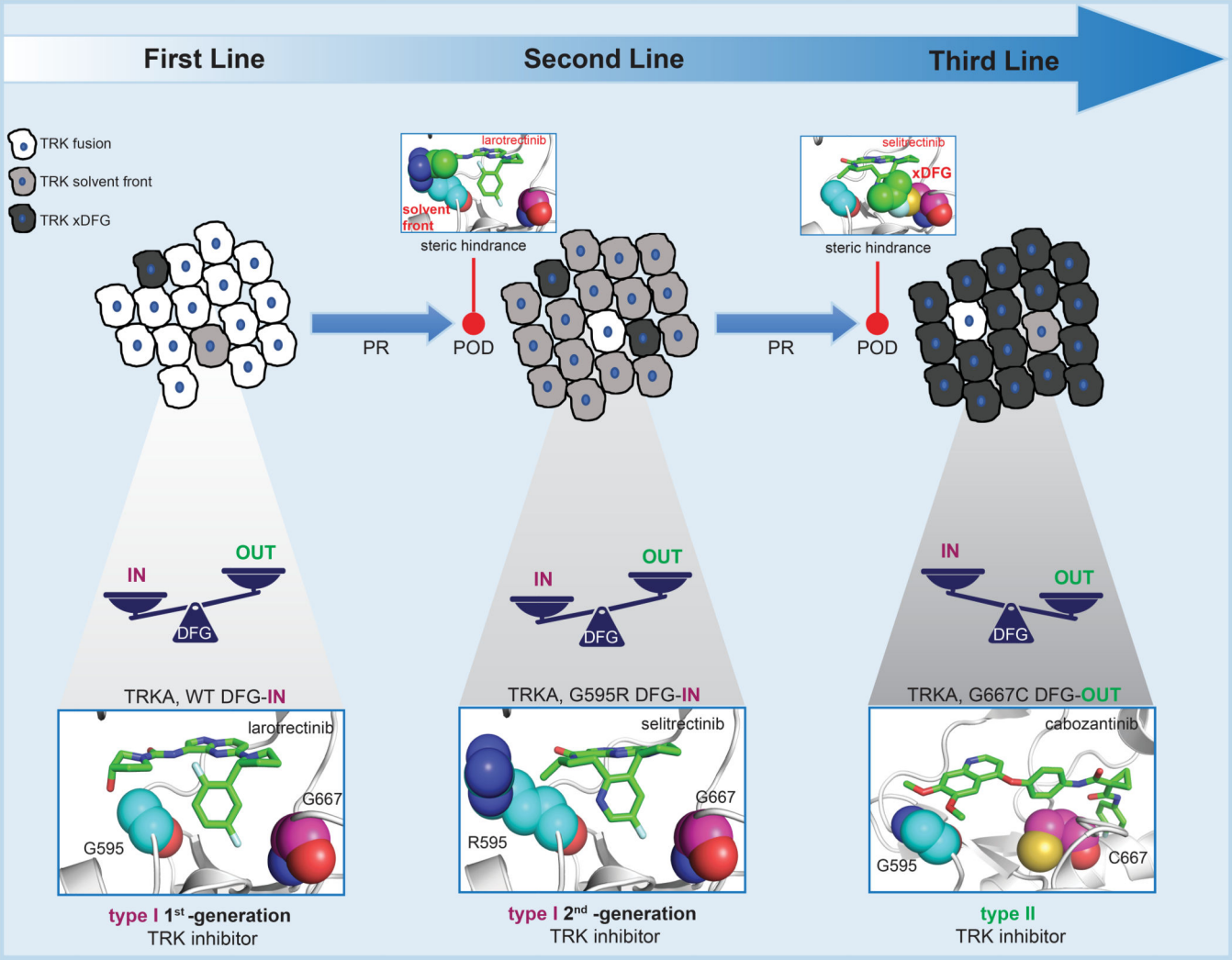

Figure 6. Proposed Model

Proposed model of sequential therapy in *NTRK* fusion-positive tumors. At diagnosis, tumors are mainly composed by WT TRK fusion-positive cells. The pool of kinase molecules in DFG-IN conformation is prevalent and patients are treated with type I, 1st-generation TRK inhibitors (first line therapy: i.e., larotrectinib). At progression, the most prevalent mechanism of on-target resistance is the emergence of TRK solvent front mutations that generate steric hindrance, thus compromising 1st-generation drugs activity. In cells harboring TRK solvent front mutations the pool of DFG-IN kinase molecules is still predominant, and patients are treated with type I 2nd-generation TRK inhibitors (second line therapy: i.e., selitrectinib). At progression, emergence of TRK xDFG single and double mutations generates steric hindrance, compromising the binding of type I 2nd-generation TRK inhibitors, and induces the kinase to preferentially adopt its inactive DFG-OUT conformation, sensitizing to type II kinase inhibitors (proposed third line therapy). Note that only on-target mechanisms of resistance are displayed in this model.